Supplement of Hydrol. Earth Syst. Sci., 30, 6927–6961, 2026
https://doi.org/10.5194/hess-30-6927-2026-supplement
© Author(s) 2026. CC BY 4.0 License.



Hydrology and Earth System Sciences
Open Access
EGU

Supplement of

Evaluation of sub-daily precipitation variability and its diurnal characteristics in satellite and reanalysis datasets against ground-based observations

Gyuyeon Choi et al.

Correspondence to: Eunkyo Seo (eseo@pknu.ac.kr)

The copyright of individual parts of the supplement might differ from the article licence.

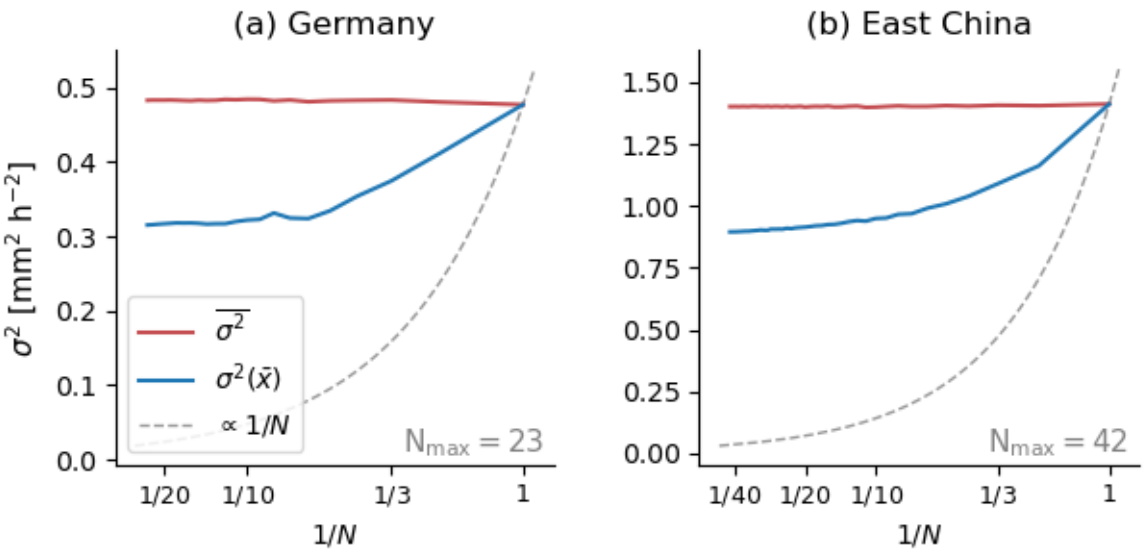


Figure S1: Sensitivity of the grid-cell averaged sub-daily precipitation variance (σ^2) to the number of stations (N), evaluated at single representative 0.5° × 0.625° grid cells in (a) Germany (51.0°N, 10.0°E), and (b) East China (31.5°N, 110.8°E). For each N from 1 to N_{max}, all possible combinations of station subset are used to compute σ^2 under two approaches: ($\overline{\sigma^2}$) in which variance is computed at each station individually and subsequently averaged across the selected stations (red line); and $\sigma^2(\bar{x})$, in which station time series are first spatially averaged and variance is subsequently computed from the resulting mean time series (blue line). The dashed line indicates the theoretical 1/N scaling expected when variance decreases solely as a result of averaging independent samples.

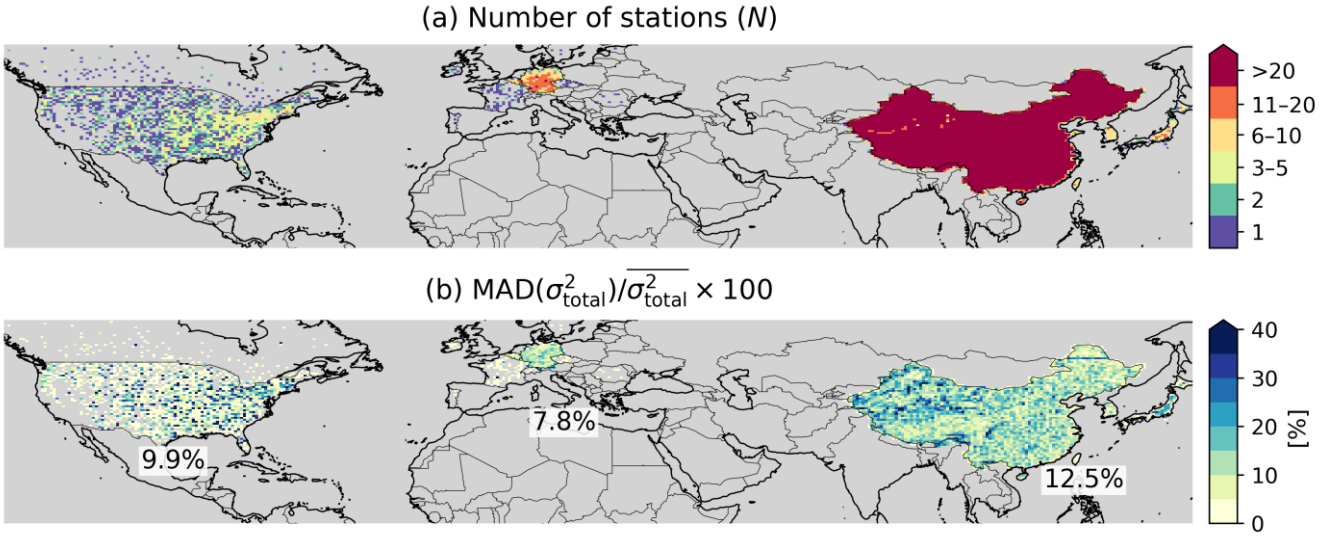


Figure S2: (a) Number of ground-based stations contained in each 0.5°×0.625° grid cell. (b) Mean absolute deviation (MAD) of the station-level total precipitation variance (σ^2_{total}) from the grid-cell mean, normalised by that mean. Number indicate the regional averages over North Americal, Europe, and East Asia.

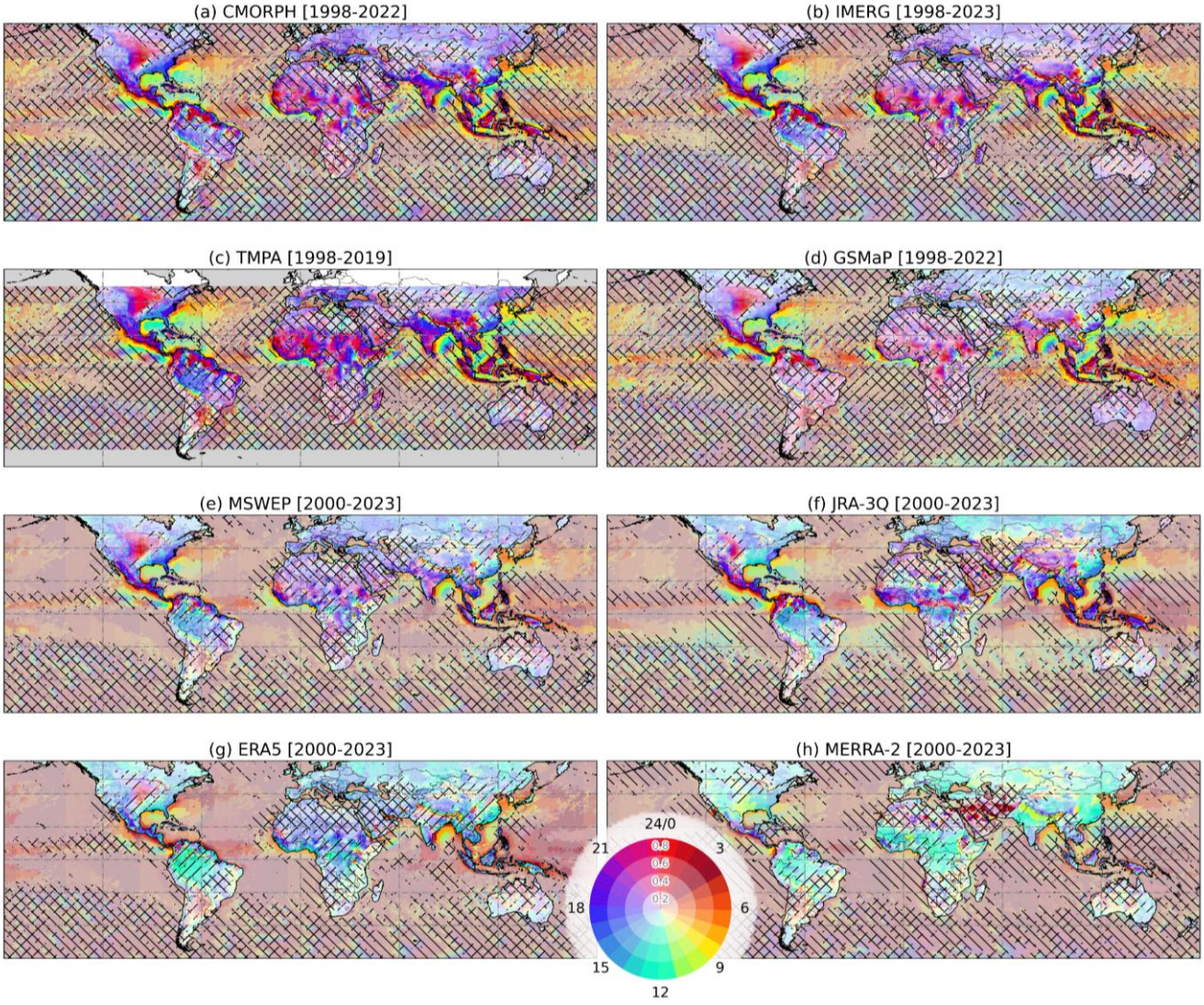


Figure S3: Same as Fig. 9a, b, but for the individual datasets (a) CMORPH, (b) IMERG, (c) TMPA, (d) GSMaP, (e) MSWEP, (f) JRA-3Q, (g) ERA5 and (h) MERRA-2.

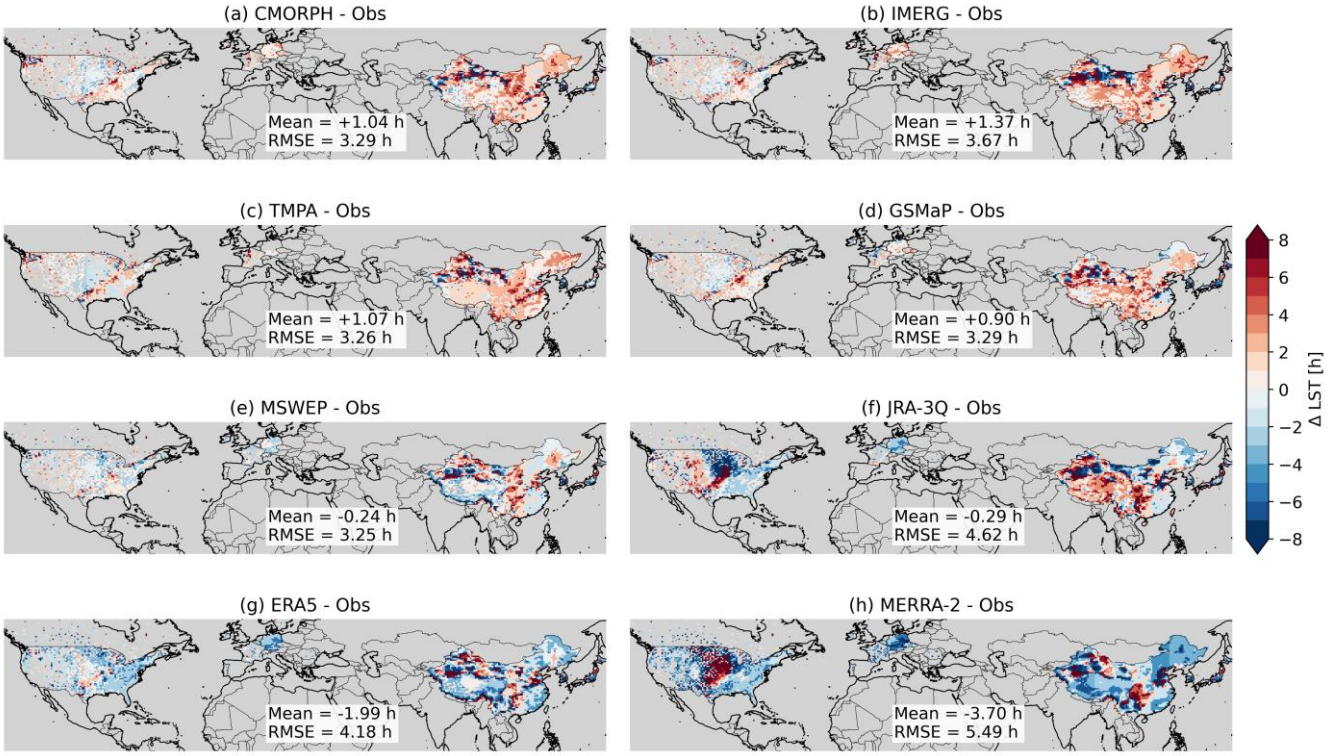


Figure S4: Same as Fig. 9c, d, but for the individual datasets (a) CMORPH, (b) IMERG, (c) TMPA, (d) GSMaP, (e) MSWEP, (f) JRA-3Q, (g) ERA5 and (h) MERRA-2.

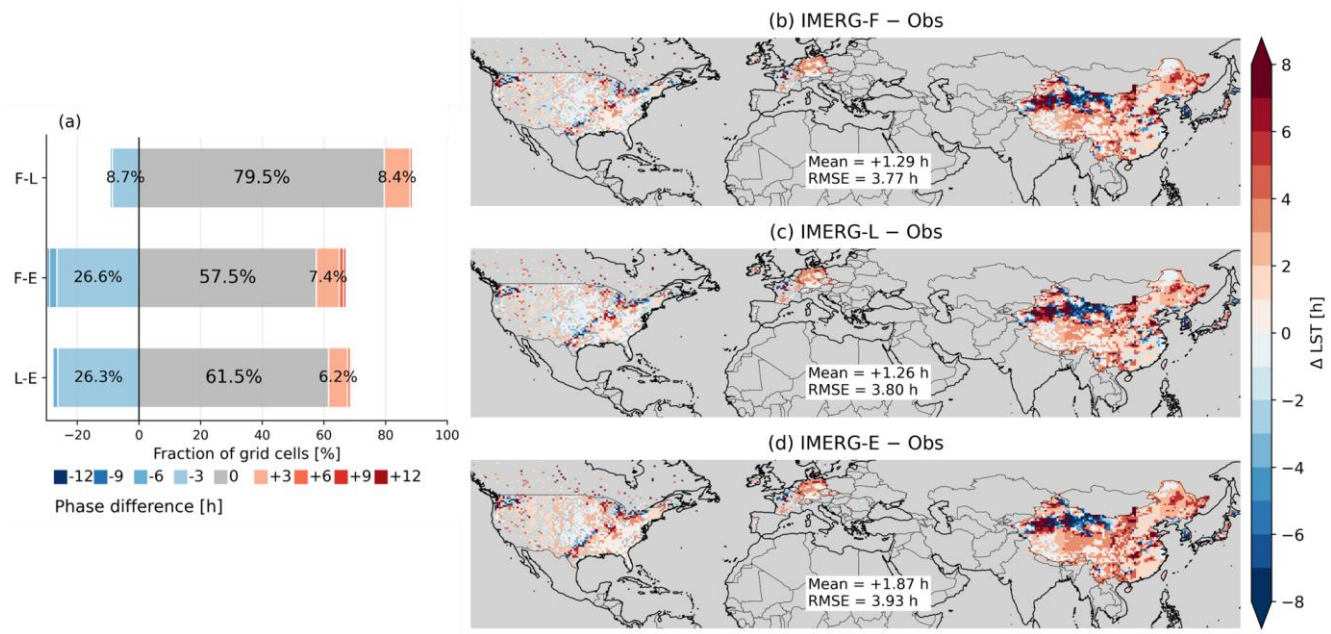


Figure S5: (a) Distribution of pairwise phase differences among IMERG-F (F), IMERG-L (L), and IMERG-E (E) over the common observation grid cells. Gray indicates identical phases, while blue and red indicate negative and positive phase differences, respectively. (b–d) First-harmonic phase differences relative to the ground-based observations for IMERG-F, IMERG-L, and IMERG-E.

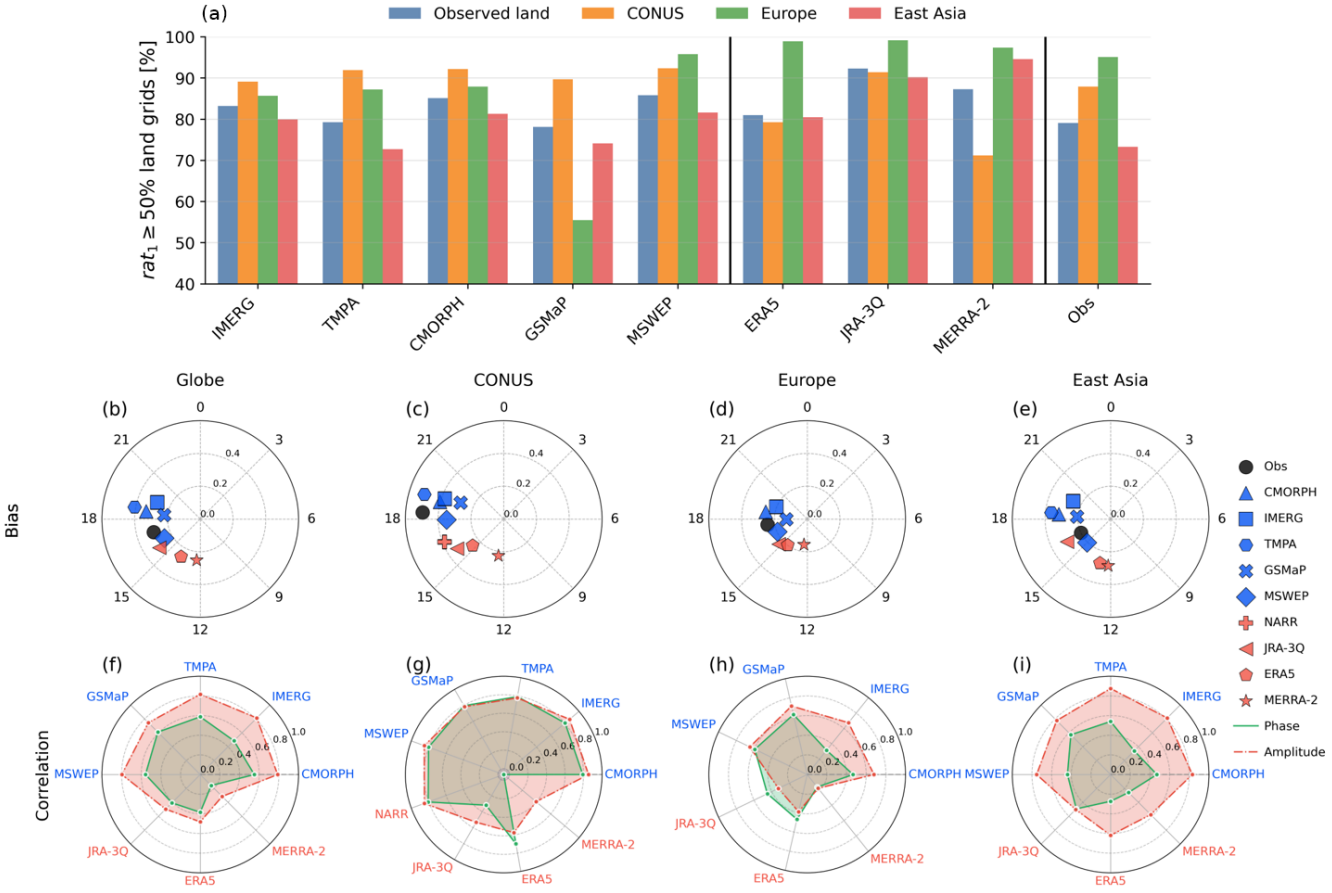


Figure S6: (a) Percentage of land grid cells with ground-based observations for which $rat_1 \geq 50\%$, given for the observed land domain as a whole (blue) and separately for CONUS (orange), Europe, and East Asia (red). (b-i) Same as Fig. 7, but without the $rat_1 \geq 50\%$ criterion, so that all grid cells with ground-based observations are included.

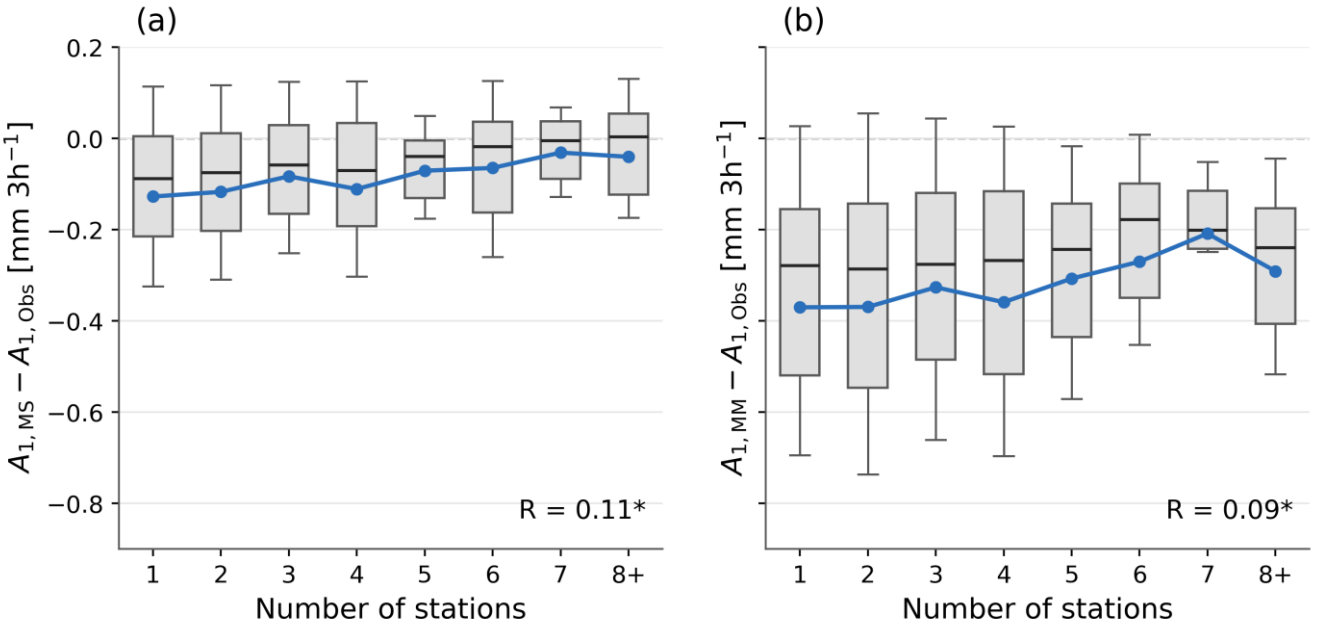


Figure S7: Differences in 1st harmonic diurnal amplitude between the gridded products and ground-based observations over CONUS as a function of the number of stations contributing to each grid cell, for (a) MS and (b) MM, where grid cells containing eight or more stations are grouped into the 8+ class. Whiskers extend to 0.5×IQR, and the blue line connects the mean difference for each station-count class. R denotes the Pearson correlation between station count and amplitude difference, with an asterisk indicating significance at the 5% level.

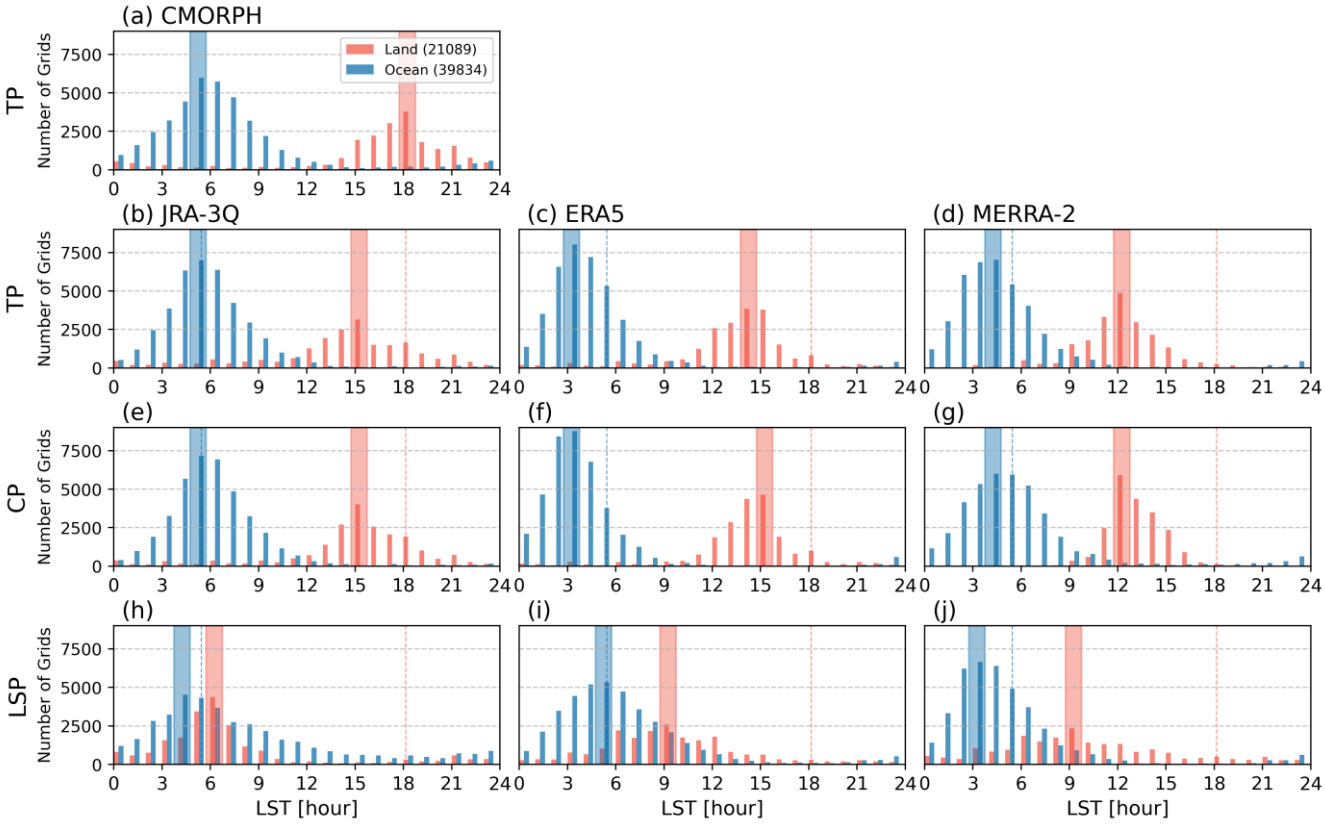


Figure S8: Histograms of the frequency distribution of the diurnal peak phase over land (red) and ocean (blue) grids bounded by 60°S–60°N (only grid point after the masking depicted in Fig. 6). (a) Total precipitation (TP) from CMORPH. For JRA-3Q (b, e, h), ERA5 (c, f, i), and MERRA-2 (d, g, j), the panels show TP (b-d), convective precipitation (CP; e-g), and large-scale precipitation (LSP; h-j), respectively. Background shaded bars indicate the local time corresponding to the maximum frequency of grid points for the diurnal peak phase.

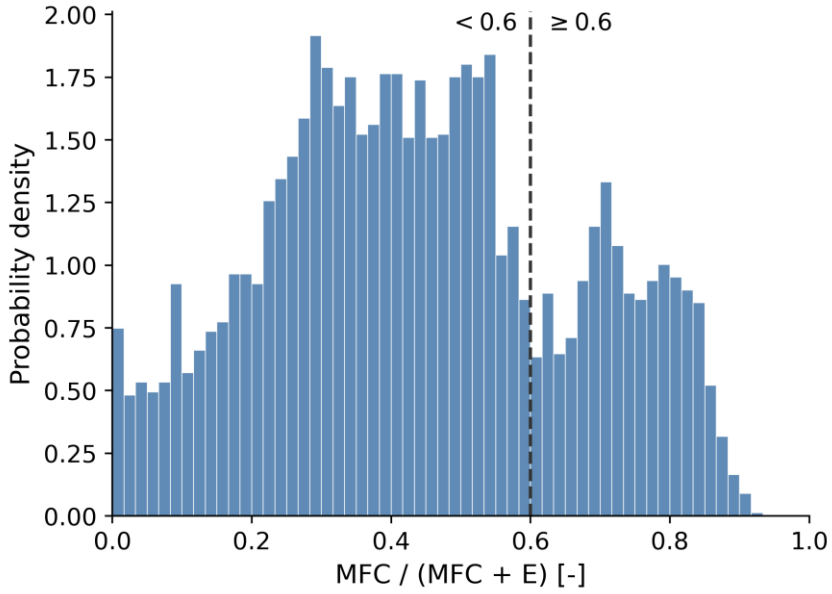


Figure S9: Probability density of the climatological daily-mean ratio MFC/(MFC+E), averaged across JRA-3Q, ERA5, and MERRA-2, over land grid cells on rainy days. The dashed line marks the threshold of 0.6 used to separate the two moisture-supply regimes.

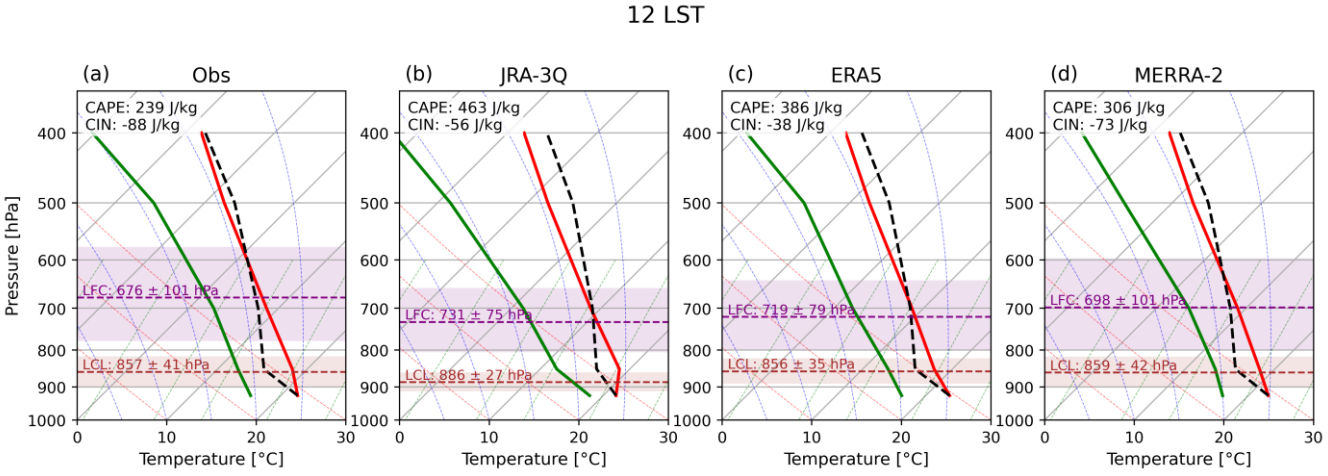


Figure S10: Mean skew-T profiles at 12 LST on rainy days at the ARM SGP site (36.6°N, 97.5°W), for (a) the IGRA radiosonde observation, (b) JRA-3Q, and (c) ERA5, and (d) MERRA-2. Red and green solid lines show temperature and dew point, and the black dashed line shows the surface-based parcel path. The brown and purple dashed lines mark the mean lifting condensation level (LCL) and level of free convection (LFC), with shading spanning ±1 standard deviation. CAPE and CIN averaged over the same profiles are given in each panel.

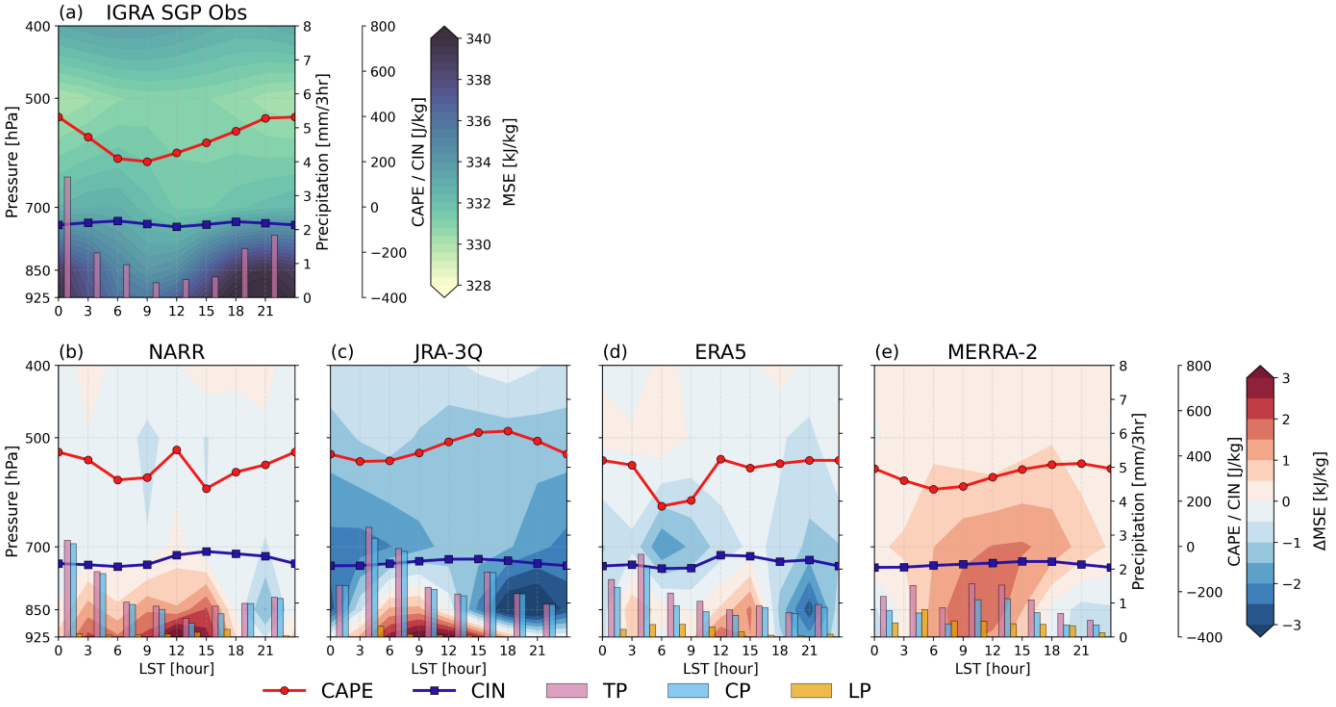


Figure S11: Diurnal variations of vertical profiles of moist static energy (MSE) from (a) IGRA observation, (b) NARR, (c) JRA-3Q, (d) ERA5, and (e) MERRA-2 at ARM SGP site (Lamont, Oklahoma; 36.6°N, 97.5°W), but reanalysis datasets show the bias of MSE (bottom row). In each panel, bar represents total (red), convective (blue), and large-scale (yellow) precipitation and red and blue lines indicate CAPE and CIN, respectively.